FLIGHT RESULTS FROM THE CANX-4 AND CANX-5 FORMATION FLYING MISSION

Niels H. Roth,[*] Ben Risi,[†] and Robert E. Zee[‡]

The CanX-4 and CanX-5 nanosatellite formation flying mission was launched on June 30 2014 from Sriharikota India on board the Polar Satellite Launch Vehicle. Just four months after launch, the spacecraft had successfully completed their mission – to demonstrate sub-metre control and centimeter-level relative positioning in along-track orbit and projected circular orbit formations ranging from 1 km to 50 m in size. In doing so the spacecraft became the first nanosatellites to demonstrate this level of performance. This work provides an overview of the innovative subsystems that enabled formation flight, in addition to a detailed discussion of the real-time navigation and control accuracy achieved during the mission.

INTRODUCTION

The use of multiple autonomously coordinated spacecraft is a critical capability to the future of spaceflight. Exciting formation flight applications include synthetic aperture radar,[1] optical interferometry, on-orbit servicing of other spacecraft, gravitational and magnetic field science,[2,3,4] geolocation,[5] and change detection such as ground-target moving indication. Groups of small, relatively simple spacecraft can also potentially replace single large and complex ones, reducing risk through distribution of instruments, and cost by leveraging non-recurring engineering costs. Performance of the entire formation can be gradually built up over several launches, maintained over time with replacement units when others fail, or allowed to degrade gracefully. Spacecraft formations also enable new types of science missions or communication systems that are not realizable with monolithic spacecraft systems.

The benefits of formation flight are best realized as the size of spacecraft decreases, nanosatellites being the foremost example. These spacecraft are cost-effective, easily mass-produced, and capable of being deployed en-masse from a single launch. It is important to note that many of the potential applications require accurate knowledge of the relative state of the system and precise relative positioning. The current state-of-the-art for autonomous formation control and relative navigation for microsatellites was demonstrated during the PRISMA mission, with control errors as low as 2 metres up to about 50 metres, and a relative navigation solution accuracy from

[*] Senior Research Associate, Space Flight Laboratory, University of Toronto Institute for Aerospace Studies, 4925 Dufferin St., Toronto, Ontario, Canada, M3H 5T6.
[†] Research Associate, Space Flight Laboratory, University of Toronto Institute for Aerospace Studies, 4925 Dufferin St., Toronto, Ontario, Canada, M3H 5T6.
[‡] Director, Space Flight Laboratory, University of Toronto Institute for Aerospace Studies, 4925 Dufferin St., Toronto, Ontario, Canada, M3H 5T6.

5 to 17 cm, depending on control input frequency.[6] Nanosatellite technology has already matured to the point where similar or better control and determination performance is possible, and at present there are several interesting and exciting missions both proposed and in development.[7] However, there had been no successful demonstrations of formation flight with sub-metre control and centimetre-level relative position knowledge with spacecraft of this scale prior to CanX–4 and CanX–5.

The spacecraft were launched on 30 June 2014 from Sriharikota, India on board the Polar Satellite Launch Vehicle (PSLV). CanX–4 and CanX–5 were deployed separately, each from its own "jack-in-the-box" style separation system. After verifying the health of both spacecraft, the attitude control systems were commissioned over the next three weeks in preparation for drift recovery. Between late July and early September 2014 a series of drift recovery maneuvers were executed to first arrest the relative drift rate of 95 km/day and then bring the spacecraft within communications range of each other. This was accomplished using the Drift Recovery and Station Keeping (DRASTK) software developed at SFL.[8] The spacecraft were then kept in safe relative orbits for a few weeks using uploaded thrust commands computed by DRASTK as formation flying and relative navigation systems were commissioned prior to the start of the fine formation control experiments in early October 2014. With full mission success in these experiments the spacecraft have set a precedent for the accuracy of relative navigation and control achievable with a nanosatellite system.

Table 1. Fine formation control experiment timeline.

Date	Formation	Notes
01 Oct. 2014	1000 m ATO	First formation control test. Sub-metre control error 88% of the time; RMS control error 0.81 m. Revised attitude targeting to improve performance.
15 Oct. 2014	500 m ATO	Sub-metre control error 100% of the time; RMS control error 0.51 m.
21 Oct. 2014	100 m PCO	Sub-metre control error 100% of the time; RMS control error 0.60 m.
02 Nov. 2014	50 m PCO	Sub-metre control error 100% of the time; RMS control error 0.59 m.
06 Nov. 2014	1000 m ATO	Sub-metre control error 100% of the time; RMS control error 0.45 m.

The timeline of the fine formation flying experiments is shown in Table 1. After revising the attitude targeting performance following the first control test, the mission's control objectives were fully met in each subsequent control experiment.

SYSTEM OVERVIEW

The CanX–4 and CanX–5 spacecraft are each approximately 6.5 kg nanosatellites based on the SFL Generic Nanosatellite Bus (GNB) architecture. The GNB structure is a 20 cm cube, designed to interface with the SFL XPOD separation system. The GNB platform (Figure 1) was designed with mission flexibility in mind. It is the basis for several existing and upcoming missions. In particular, the GNB platform has been used for the BRIght Target Explorer (BRITE) constellation of stellar astronomy spacecraft, consisting of five operational satellites;[9] ExactView–9, a ship-tracking mission,[10] and the ship-tracking AISSat constellation,[11] consisting of two operational satellites on-orbit and a third slated for launch later this year. Both CanX–4 and CanX–5 are identical to each other in design. The CanX–4 and CanX–5 spacecraft layout is illustrated in Figure 2.

For downlink, CanX–4&5 use an S-band transmitter connected to two wide-beam S-band patch antennas, mounted on opposite faces to provide near-omnidirectional coverage, with downlink speeds between 32 kbps and 256 kbps. Command uplink is implemented via a UHF receiver

with a canted turnstile antenna system, also providing near omnidirectional coverage. This overall communications approach avoids so-called "death modes" in the communications system, allowing spacecraft communications in all attitudes. During autonomous formation flight, data is passed between the spacecraft using an S-band inter-satellite link (ISL), which has a demonstrated range exceeding 100 km with an omnidirectional antenna system.

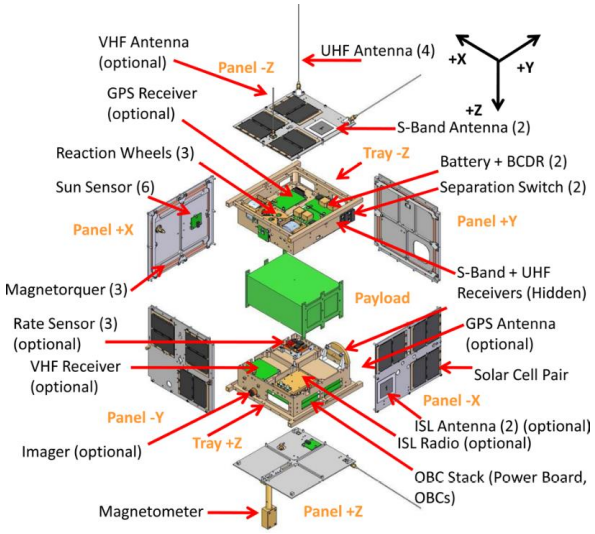

Figure 1. Exploded View of the SFL Generic Nanosatellite Bus (GNB).

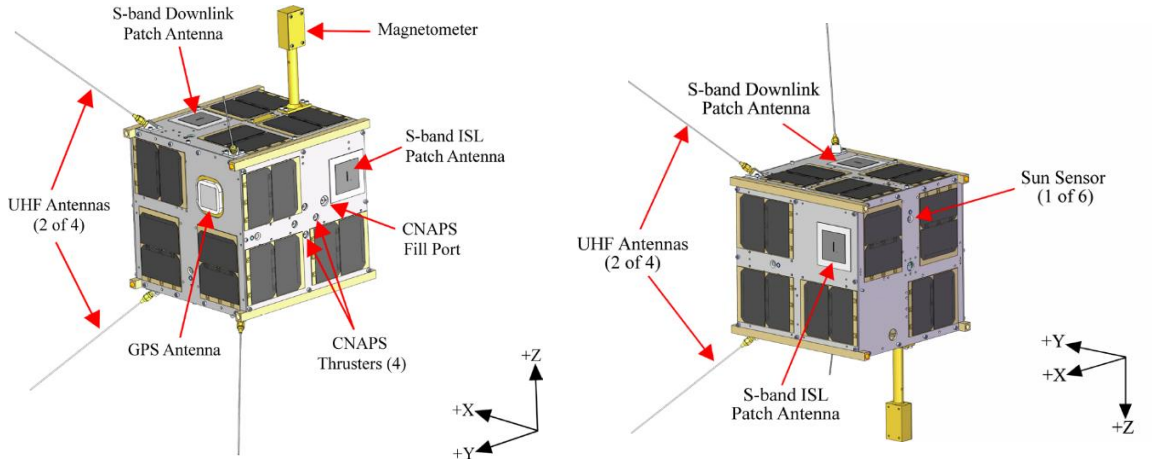

Figure 2. CanX-4 Spacecraft (CanX-5 Identical).

As with all GNB spacecraft, CanX–4 and CanX–5 each carry a suite of attitude sensors and actuators for full three-axis attitude determination and control. These include six fine sun sensors, a three-axis rate sensor, a three-axis magnetometer mounted on an external pre-deployed boom, and three sets of orthogonally mounted magnetorquers and reaction wheels. An SFL-qualified commercial off the shelf GPS receiver and active L1 antenna are used to collect high precision information on spacecraft position.

Intersatellite Link

The intersatellite link (ISL) radio enables autonomous on-orbit communications between the two spacecraft. The ISL is a compact, medium-range, low-data-rate S-band radio link. Each spacecraft is equipped with a radio module (Figure 3) and two dedicated patch antennas. The ISL provides the timely and reliable bi-directional exchange of data messages between the two spacecraft at distances up to 5 km and data rates up to 10 kbps.

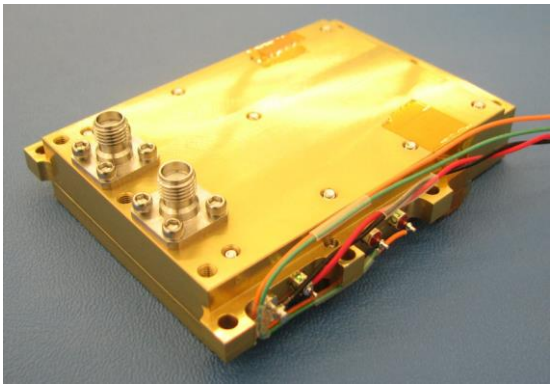

Figure 3. ISL Radio Module.

The ISL consumes 400 mW of power when receiving and 600 mW of power during transmission. It provides 21.8 dBm of RF output power to the antennas, which emit 15.3 dBm of equivalent isotropically radiated power. With the measured antenna gains, simulations showed that a link availability of greater than 98% is achievable during formation flight, and better than 90% availability at the 5 km maximum design distance.[12] It should be noted that the ISL firmware is upgradeable, allowing implementation and testing of different protocol stacks.

Propulsion

The Canadian Nanosatellite Advanced Propulsion System (CNAPS) cold gas propulsion system provides orbital control for drift recovery, station keeping, and formation control and reconfiguration (Figure 4). CNAPS is equipped with four thrusters and fueled with 260 g of liquid sulfur hexafluoride (SF_6) propellant, providing a specific impulse of 45 s and a total ΔV capability of 16 m/s. SF_6 was chosen for its high storage density and vapour pressure which makes the system self-pressurizing, as well as its inert properties, making it both safe to handle and compatible with most materials.[13] CNAPS is the largest payload on board the CanX-4 and CanX-5 spacecraft with a volume of 7 cm × 12.5 cm × 18 cm. Two filters are present in the system to remove any contaminants that could damage the solenoid valves, and a pressure relief valve on the storage tank is used to ensure against the possibility of an overpressure event compromising safety on the ground or the launch vehicle. Thrust levels range from 12.5 to 50 mN, depending on thruster selection. As the four nozzles are located on a single face of the spacecraft bus, thruster selection also allows the system to be used for momentum management, with specific nozzles autonomously selected to reduce momentum build-up on the reaction wheels. Having only one axis of thrust requires that the attitude control system be able to quickly slew the spacecraft during formation flight, such that the thrusters point in the correct direction prior to thrusting.

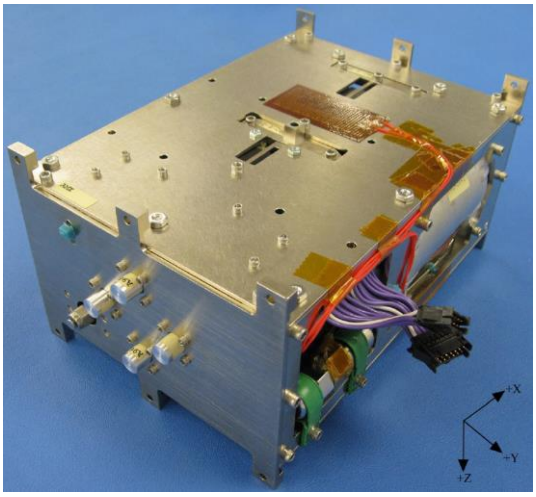

Figure 4. CNAPS Propulsion Flight Unit for the CanX-4 Spacecraft.[13]

MISSION OVERVIEW

Spacecraft formation flight can be defined as the active control of the relative separation between two or more spacecraft. Here one spacecraft, designated the Chief, is uncontrolled and serves as the reference while the second spacecraft, designated the Deputy, performs active control to maintain a prescribed relative motion with respect to the Chief.

The main goal of the mission is to demonstrate precise autonomous formation flight with control error less than 1 m (2σ) in four formations with a minimum duration of 10 orbits each. The two formation types are the along-track orbit (ATO) and the projected-circular orbit (PCO). The ATO can be thought of as a "leader-follower" configuration, where one spacecraft is simply offset in mean anomaly. The PCO is designed such that as viewed from Earth, one satellite appears to encircle the other once per orbit. The four formations are selected to be a 1000 m ATO, a 500 m ATO, a 100 m PCO, and a 50 m PCO. These formation reference trajectories are given by the periodic solutions to Hill-Clohessy-Wiltshire (HCW) equations of relative motion[14]

$$\begin{aligned} x(t) &= \frac{d_1}{2}\sin(nt+\alpha) \\ y(t) &= d_1\cos(nt+\alpha)+d_3 \\ z(t) &= d_2\sin(nt+\beta) \end{aligned} \tag{1}$$

where n is the Chief spacecraft's mean orbital angular velocity, and the constants d_1, d_2, d_3, α and β are formation design parameters. The relative position of the Deputy with respect to the Chief given by $x(t)$, $y(t)$, and $z(t)$ is expressed in the local-vertical local-horizontal reference frame of the Chief. This frame, also known as the Hill frame or the orbit frame, has its x-axis defined as the normalized Chief position vector, its z-axis defined as the normalized Chief angular velocity vector, with the y-axis completing the orthonormal triad. The X, Y, and Z directions are sometimes referred to as the radial, along-track or tangential, and cross-track or normal directions. The relative motion in the cross-track direction is decoupled from the other two axes – a fact that is used to create passively safe relative orbits by ensuring that the radial and cross-track motions are out of phase and are thus never simultaneously zero. The formation design parameters are given in Table 2. Note that the ATO formations are designed with passive safety in mind to ensure that

the spacecraft will not collide if they fall out of formation and begin drifting along-track. Unfortunately it is not possible to achieve a passively safe configuration with the PCO geometry.

Table 2. Formation design parameters.

Formation	d_1 (m)	d_2 (m)	d_3 (m)	α (°)	β (°)	Duration (orbits)
ATO 1000	60	30	1000	0	90	11
ATO 500	60	30	500	0	90	11
PCO 100	100	100	0	0	0	11
PCO 50	50	50	0	270	270	11

FORMATION FLYING NAVIGATION AND CONTROL ALGORITHMS

There are three main algorithms running onboard the spacecraft that enable formation flying – the onboard attitude system software (OASYS), the formation flying integrated onboard nanosatellite algorithm (FIONA), and the relative navigation algorithm (RelNav).

OASYS performs the attitude determination and control tasks for the spacecraft. It runs on the attitude determination and control computer (ADCC) of each spacecraft at a two second period. Attitude state estimation is performed using an extended Kalman filter which incorporates measurements from the magnetometer, sun sensors, rate gyro, and reaction wheels to estimate the inertial to body quaternion and angular velocity. The reference trajectory is either an inertial attitude, or a nadir-tracking attitude with an arbitrary offset from the orbit frame. Reaction wheel momentum management is performed in parallel to the control tasks – the Chief uses magnetorquers, while the Deputy spacecraft employs intelligent thruster selection to mitigate momentum build-up. This is possible since the four thrusters are arranged surrounding the spacecraft centre of mass.

During active formation flying both spacecraft attitudes are commanded by FIONA; the target attitude is computed on the Deputy and transmitted to the Chief over the ISL. This is to ensure that both spacecraft have the same attitude. Maintaining common attitude is required to maximize the number of common GPS satellites in view to improve relative state estimation. The target attitude is computed to align the thrust axis with the desired inertial direction while simultaneously constraining the GPS antenna boresight to zenith, which maximizes view of the GPS constellation. OASYS is also programmed to autonomously revert to a zenith-tracking attitude if no new thrust commands are received for a predefined period of time. This helps improve relative state estimation between thrust periods. To enable formation flying, the attitude control system must be capable of reorienting the spacecraft up to 180 degrees in 60 seconds – the minimum time between control thrusts. At the end of the maneuver the thrust axis pointing error must be less than 6° and the angular rate perpendicular to the thrust axis less than 0.3°/s, otherwise the formation control thrust is not executed.

FIONA is the formation control software running on the Deputy POBC – given a relative state estimate, it computes the required control thrust time and magnitude, along with the required target attitude. FIONA also has an extended Kalman filter for smoothing absolute GPS state estimates and provides coordinate transformations for mapping the relative state estimate from the Earth-centered Earth-fixed frame to the Hill frame as required by the control laws. There are two main modes of operation – reconfiguration mode and formation control mode. Thrust targets and attitude commands are always computed, but whether or not they are acted upon can be controlled through a set of flags: passive (no commands), attitude active (only attitude commanded),

and orbit active (attitude and thrust commanded). This method of operation was found to be very useful during commissioning.

In reconfiguration mode a set of thrusts is computed to bring the spacecraft from one relative state to another at a prescribed point in time. The reconfiguration start and end times are fixed (configurable by the operator), and a configurable number of thrusts are distributed evenly in time between the end points. The thrusts (ΔV's) are computed as the closed-form solution to the problem of minimizing the reconfiguration energy while establishing the final desired state subject to the relative motion dynamics as described by a state transition matrix.[15] Configurable limits are defined for the maximum ΔV per maneuver and maximum reconfiguration ΔV to prevent arbitrarily large reconfigurations being attempted. A new set of thrusts is computed following each executed thrust until only one thrust remains. This closed-loop reconfiguration method was found to be far more robust and accurate in the presence of thrust errors, pointing errors, and relative state estimation errors.

The formation control mode computes control thrusts required to track a reference trajectory as described by Equation (1). The controller is a continuous linear quadratic regulator formulated using the error dynamics of the equations of relative motion.[16] Such a formulation is possible since the desired trajectories are natural solutions to the equations of relative motion. The control acceleration computed by the LQR is converted to an impulse using the LQR control period of 75 seconds. Since the spacecraft have just one axis of thrust, 60 seconds of the control period is allotted for reorienting the thrust axis with ten seconds for thrusting. The computed control impulse is saturated such that CNAPS is never required to be active longer than 15 seconds. This ensures that the system will always be capable of performing the required orbit corrections.

RelNav is the workhorse of the formation flying algorithms and has by far the greatest computational complexity. It runs only on the Deputy POBC. Its task is to provide accurate relative position and velocity estimates to be used in the formation control algorithms. The accuracy of the relative velocity estimate is paramount, since it is directly related to fuel consumption and formation control accuracy. RelNav's design is adapted from several sources (References 17, 18, 19, 20, 21, and 22), and its details can be found in Reference 15. RelNav is an extended Kalman filter that estimates the relative position and velocity of the Deputy with respect to the Chief using single-difference (SD) pseudorange and carrier phase measurements from all commonly tracked GPS satellites. The state vector is augmented with differential GPS clock bias and clock bias drift as well as the float SD carrier phase ambiguities. The state vector size changes dynamically with each cycle, since the commonly tracked satellites change frequently. The relative orbital state is propagated forward in time using "pseudo-relative" dynamics as in Reference 21 with a degree and order 6 Earth gravity model; the contributions of higher order effects such as third-body perturbations, and differential drag are safely neglected given the close relative separation and common spacecraft design.

FORMATION FLYING COMMISSIONING RESULTS

Prior to commencing autonomous formation flight, it was required to commission the subsystems and algorithms to ensure that they were performing as expected when compared with offline simulations. Here we focus on the results of an important experiment performed on September 18, 2014. In this test, the spacecraft were commanded with a pre-programmed time sequence of attitude targets representative of those expected during fine formation flying. One orbit's worth of targets were programmed for each formation – 80 for the ATO (from 17:21:00 to 19:00:30) and 80 for the PCO (from 20:18:00 to 21:57:30), spaced at 75 s intervals. There were two main goals of the experiment: first, to verify that the attitude control systems were capable of meeting

the targets with sufficient speed and accuracy, and second to ensure that the onboard relative navigation algorithm is able to deal with the frequent changes in GPS satellites tracked.

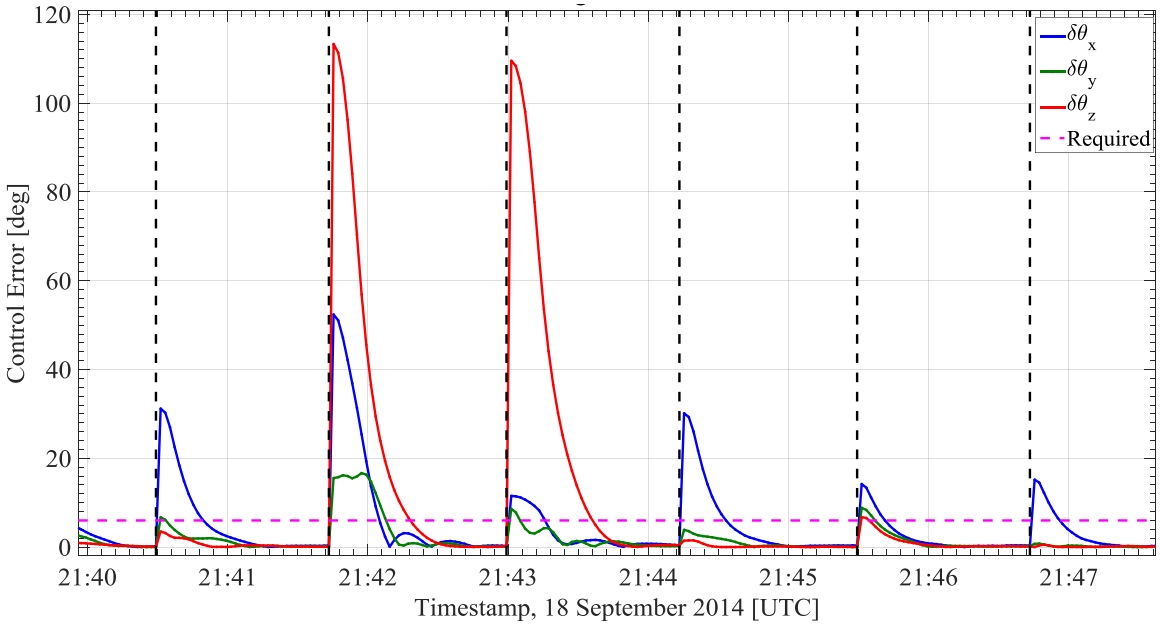

Figure 5. Attitude control error (3-2-1 Euler angle sequence) for 6 target attitudes during the PCO target test on CanX-5. The dashed black lines represent new attitude targets.

For each commanded attitude, the thrust axis pointing error and angular velocity perpendicular to the thrust axis are computed after 60 s, or 30 attitude control cycles. Recall that the required thrust axis pointing error must be less than 6° and the angular rate less than 0.3°/s after one minute, otherwise the thrust would not be executed during fine formation flying. An example of CanX-5's control performance is shown in Figure 5. Here we are more concerned with errors about the Y and Z axes than about X, since Y and Z correspond to thrust axis pointing errors, while errors about X correspond to pointing the GPS antenna towards zenith. The maneuvers at 21:42 and 21:43 are the two largest thrust axis reorientations for the PCO test. The system responds very quickly to new attitude targets, reducing the overall control error below 2° in less than 25 control cycles. The attitude control performance in this experiment is summarized for both spacecraft in Table 3. Here we tabulate the distribution of thrust axis pointing error and off-thrust axis angular rate 60 s after the initial command is issued. An attitude target is considered to be met if the pointing and rate control errors are below the requirement after 60 s. The steady state control error was found to be well below the requirement, with 95% of the final errors having greater than 33% margin. For each test case the spacecraft missed at most one target; the success rate was well above what is required to maintain sub-metre formation control accuracy.

Table 3. Attitude Control Performance Summary - September 18 2014 Targeting Tests.

Test Case	Spacecraft	Number of Targets Achieved	Thrust Axis Pointing Error (°)			Off-Axis Rate Error Magnitude (°/s)		
			70th %ile	95th %ile	Max.	70th %ile	95th %ile	Max.
ATO Targets	CanX-4	79/80	0.49	1.72	5.12	0.04	0.14	0.43
	CanX-5	79/80	0.48	1.11	7.30	0.03	0.20	0.69
PCO Targets	CanX-4	80/80	0.49	1.02	2.81	0.04	0.14	0.29
	CanX-5	79/80	0.50	1.13	3.44	0.04	0.11	0.35

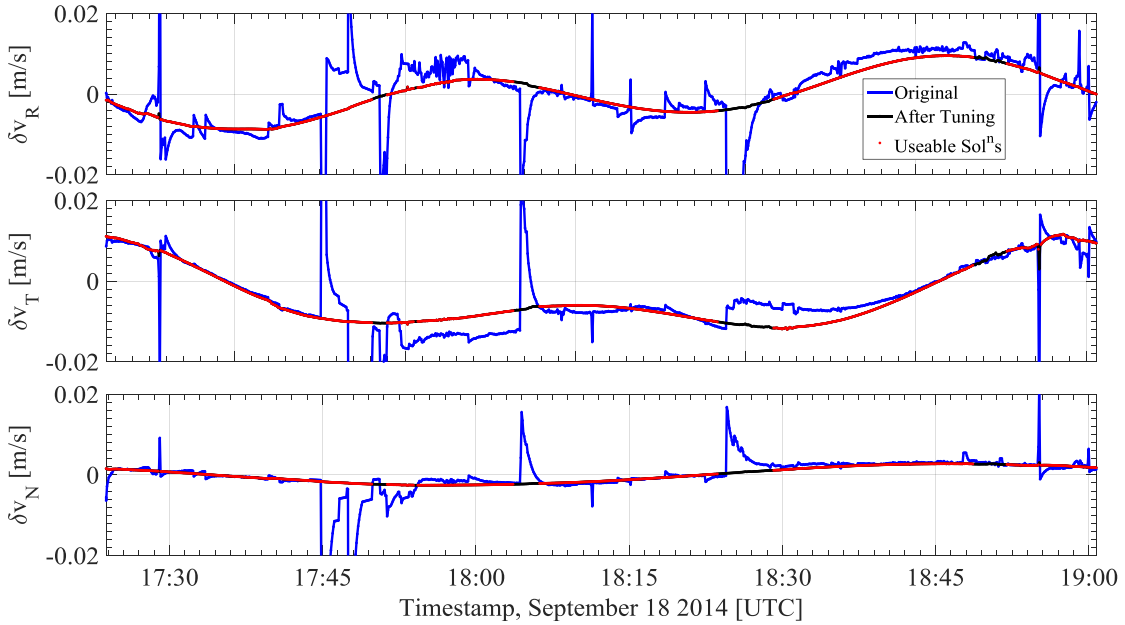

Figure 6. Estimated Relative Velocity in the Hill Frame from the ATO Target Test - Before and After Tuning.

An example of the RelNav results from the ATO target portion of the experiment is shown in Figure 6. Initially, the filter parameters from ground-based hardware-in-the-loop testing were used. The blue line shows the onboard estimate using the initial filter parameters (i.e., before tuning) to be unsatisfactory. The expected result is a smoothly varying relative velocity, since neither spacecraft was under thrust. However, RelNav erroneously reported many sudden changes in the estimated relative velocity. The primary cause of the velocity spikes was admitting all common GPS satellites into the filter, regardless of elevation with respect to the antenna boresight. The noisier measurements from these low elevation satellites were found to have a detrimental effect on the estimate. To correct this issue, the measurement pre-processing was adjusted to accept only measurements with a carrier to noise density ratio (C/N_0) above 42 dB-Hz, effectively applying an elevation mask of 20° with respect to the antenna plane. A second cause was the filter was placing a heavier weight on new measurements rather than the state propagation. This was corrected by decreasing the velocity process noise covariance. A third cause of the velocity spikes in the onboard estimate was due to intermittent communication resulting from operating the ISL radios outside their designed range of 5 km (the range during this test was 6.8 km). In certain orientations there was simply not enough gain in the system to send the required data,

leading to many openloop cycles (30 to 60% at times) and subsequent jumps in the solution when communication was restored and a whole new set of GPS satellites were in view and the new carrier phase ambiguity states had not yet converged. This was not a concern, since it was known that the ISL would have close to 100% coverage during the fine formation flying experiments.

The attitude and GPS data recorded during the experiment was downloaded and input to an offline version of RelNav. The filter parameters and settings were adjusted using the results of the offline runs until the desired performance was achieved. The post-fit measurement residuals were used as a performance metric, in addition to qualitative inspection of the relative estimates to ensure they were free of sudden jumps, or correctly reported such estimates as erroneous and thus unfit for use in the formation control algorithm. The tuned filter results are shown in black in Figure 6, with the red points denoting estimates flagged as reliable to use in formation control. The state estimate of the tuned filter was greatly improved, with the majority of the spikes being smoothed out or otherwise being flagged as unreliable. The remaining errors in relative velocity were approximately 1 mm/s, and were thus deemed acceptable for fine formation flying.

FINE FORMATION CONTROL RESULTS

In this section we first provide an overview of the experiment planning considerations, and then discuss the main formation flying navigation and control results. The formation control accuracies presented are computed using on-board RelNav estimates.

Prior to each formation control experiment, the drift recovery and station keeping (DRASTK) software developed at SFL was used to compute a set of thrusts to bring the spacecraft to within approximately 1 km of the target formation in a passively safe relative orbit.[8] The initial conditions for the maneuver computation were supplied from offline EKF/smoother state estimates using single-point GPS position and velocity solutions as measurements. Next, offline formation control simulations were performed using the expected relative state following the DRASTK maneuvers as an initial condition. The offline simulations helped establish the autonomous reconfiguration start and end points, as well as the predicted fuel consumption. The reconfigurations were timed to begin near the start of a morning pass block (the two to four communications windows each morning between the SFL ground station and CanX-4&5) with an overall duration of three or four orbits such that early progress could be monitored for the remaining morning passes. All formations were held for 11 orbits, with the final orbit planned to end before or during the next pass block. This was done so that if required, maneuvers to restore passively safe relative orbits could be applied as close to the end of the controlled formation as possible. Typically, at least two days were required to download the large volume of payload data collected. During this time DRASTK was used to re-establish a safe relative orbit prior to the next experiment.

Special considerations were required for the PCOs, since this formation can result in a collision within a few orbits if control is not actively applied. In planning the PCOs, one set of contingency thrusts for each ground contact during the formation were computed with DRASTK and prepared for upload in case it was found that the spacecraft had fallen out of formation. These thrusts were designed to establish a 90° phase offset between the radial and cross-track motions to ensure no collisions for any along-track drift. Fortunately, these maneuvers were never required.

The first formation attempt was the 1000 m ATO on October 1st. In this test the formation was autonomously acquired and control was maintained for the required 10 orbit period; however, the control error was sub-metre only 88% of the time, just below the 95.45% requirement. The ultimate cause was determined to be poor navigation performance resulting from FIONA commanding target attitudes for thrust commands below the minimum impulse bit. The spacecraft were

thus reorienting to align the thrust axis with a thrust that would never occur. This led to the GPS antennas often pointing away from zenith, resulting in less commonly tracked satellites with C/N_0 above the acceptable threshold and thus less reliable solutions. A greater number of unreliable solutions led to less control thrusts, resulting in more excursions outside the desired control window. Even so, the maximum control error during this first test was only 2.25 m, which was an excellent first result.

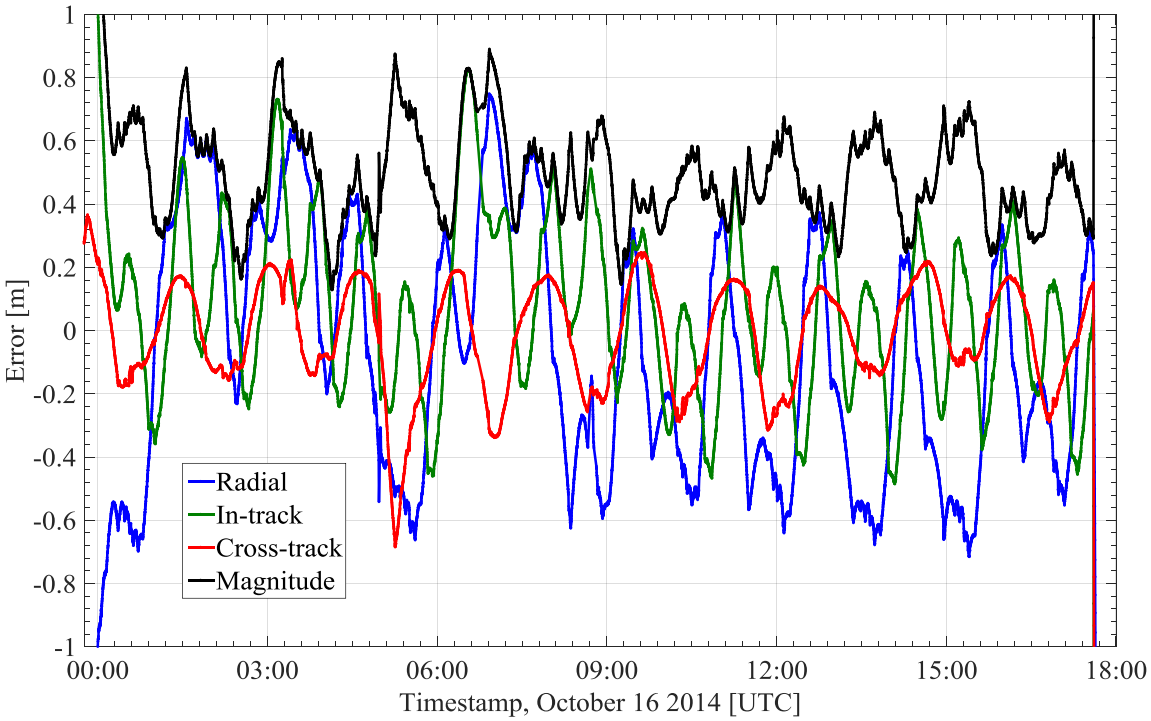

Figure 7. Formation control error during the 500 m ATO. Following the convergence period the control error remained below the 1 metre requirement.

After the root cause of the degraded navigation performance was diagnosed and corrected, new software was uploaded to the spacecraft prior to attempting the next ATO. With the attitude targeting improvements, the 500 m ATO was a complete success. The reconfiguration error was 2.9 m and 4.4 mm/s, after which it took approximately 26 minutes and 7 control thrusts to establish a sub-metre control error. As shown in Figure 7, after the initial convergence period the formation control error remained sub-metre for the duration of the experiment. The periods during which the control error is increasing correspond to times where no control thrust is applied since the desired value is below the minimum impulse bit. The mean time between control thrusts was 8 minutes and 40 seconds – far less frequent than the worst case of 75 s. The fuel consumption was 1.6 cm/s/orbit – just under the 1.7 cm/s/orbit predicted in hardware-in-the-loop tests. The set of control inputs for this formation is shown in Figure 8.

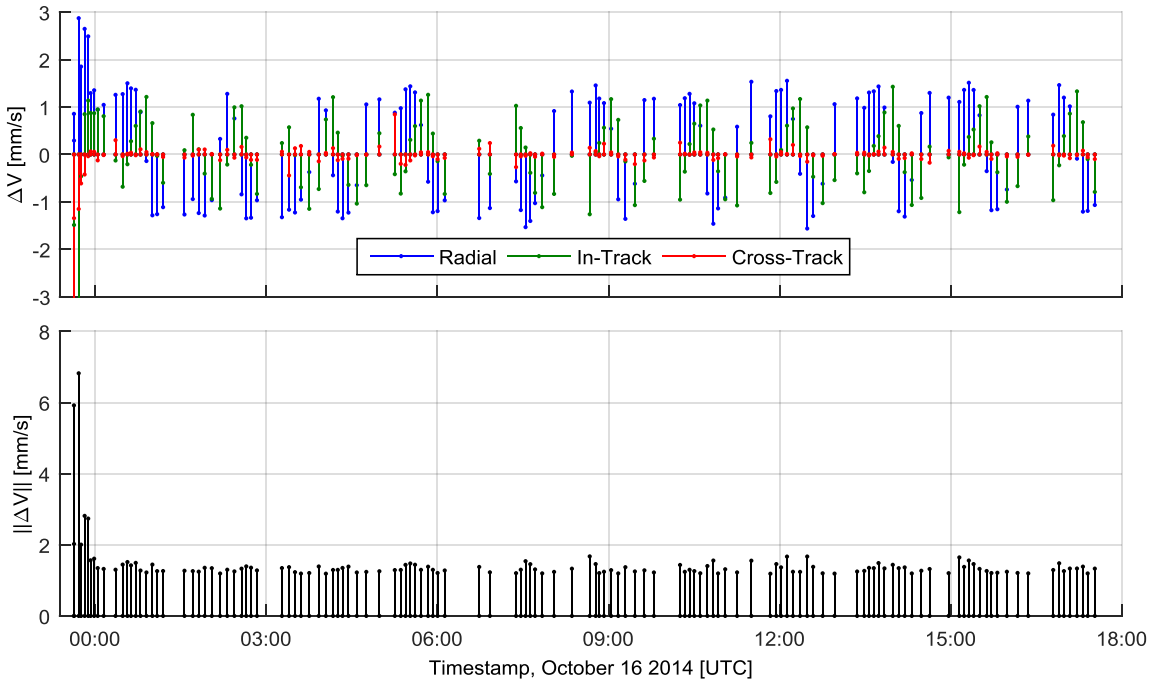

Figure 8. Control Inputs for the 500 m ATO.

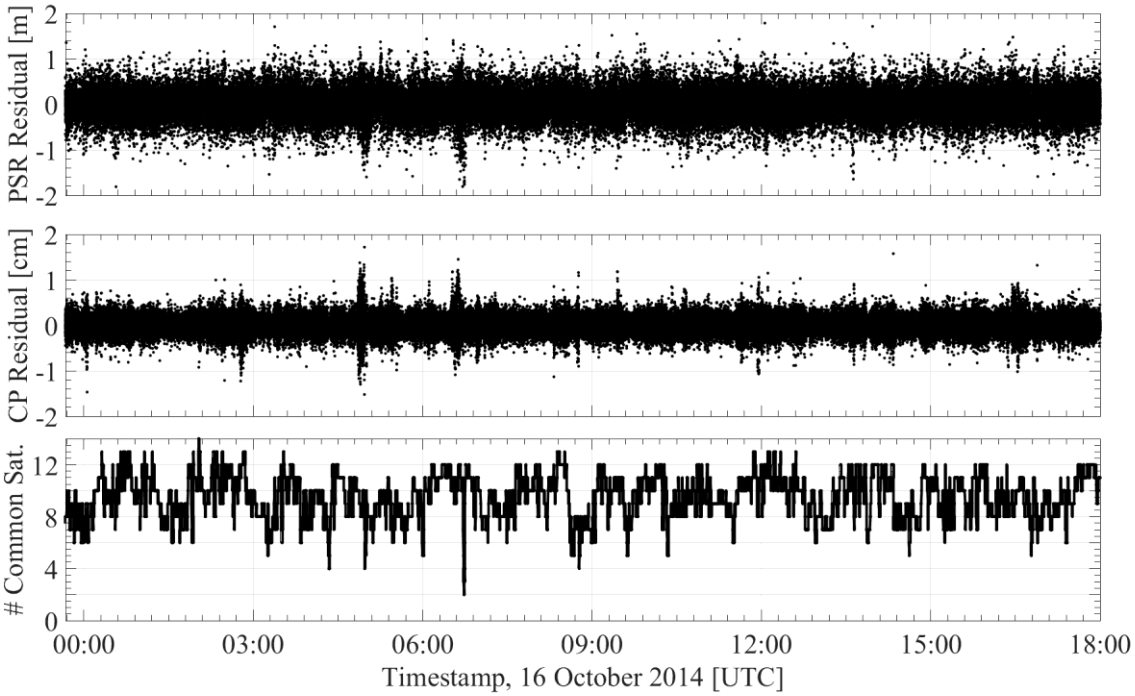

Figure 9. RelNav SD Pseudorange (PSR) and Carrier Phase (CP) Measurement Residuals.

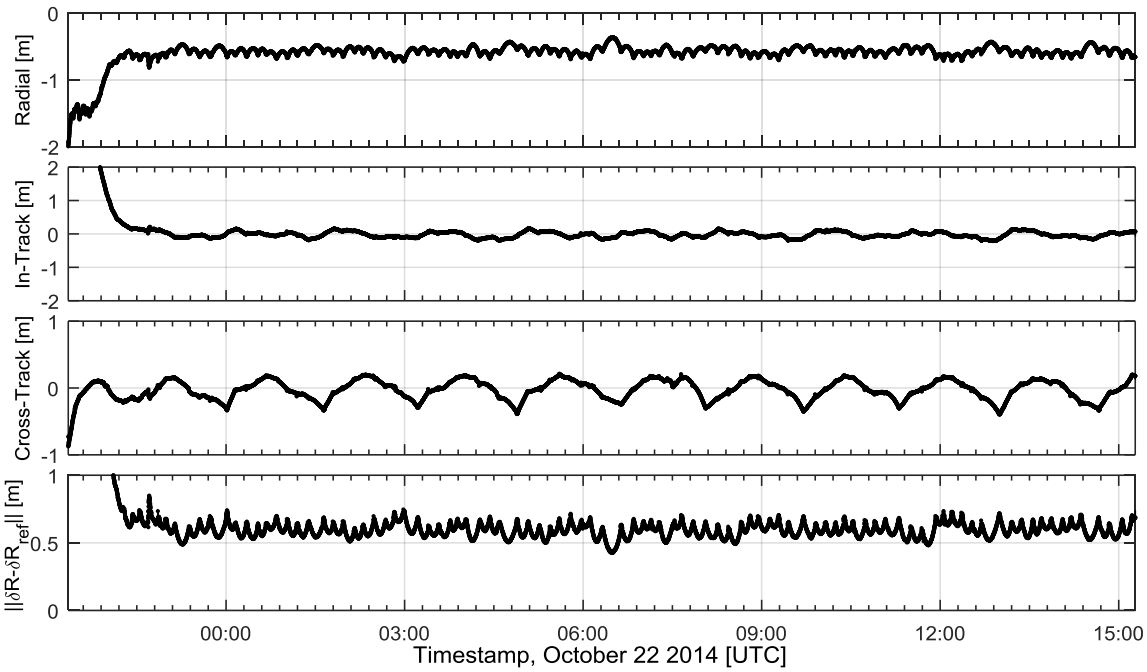

Figure 10. Control Error During the 100 m PCO.

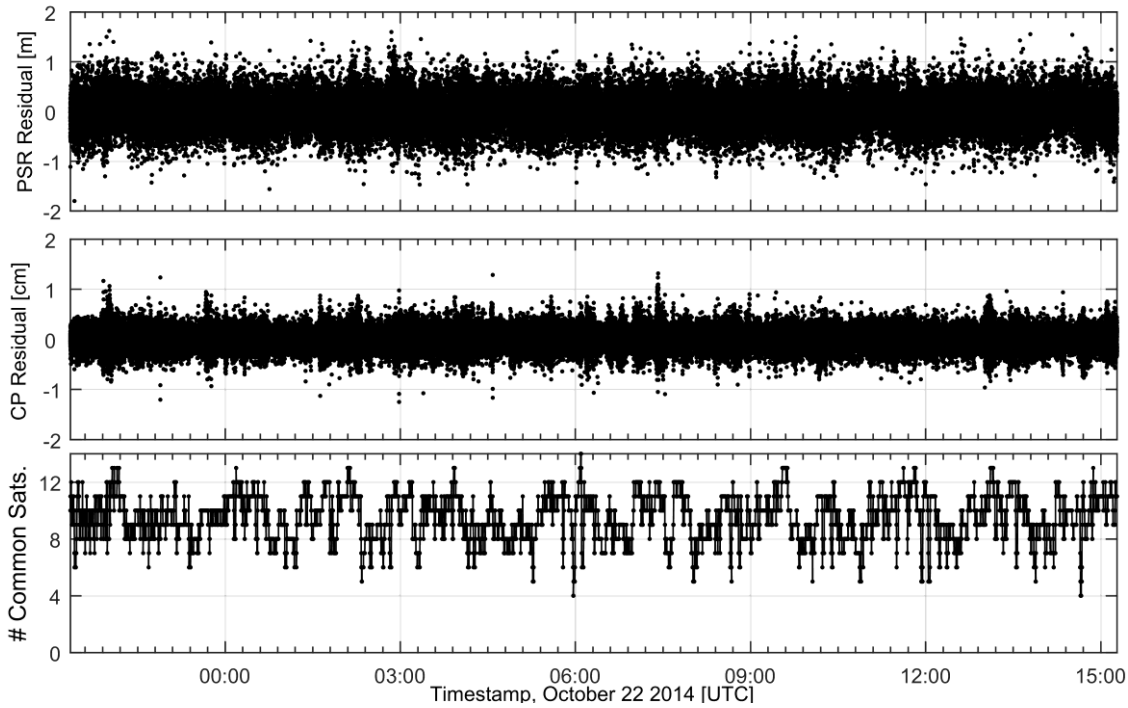

Figure 11. Post-Fit Measurement Residuals for the 100 m PCO.

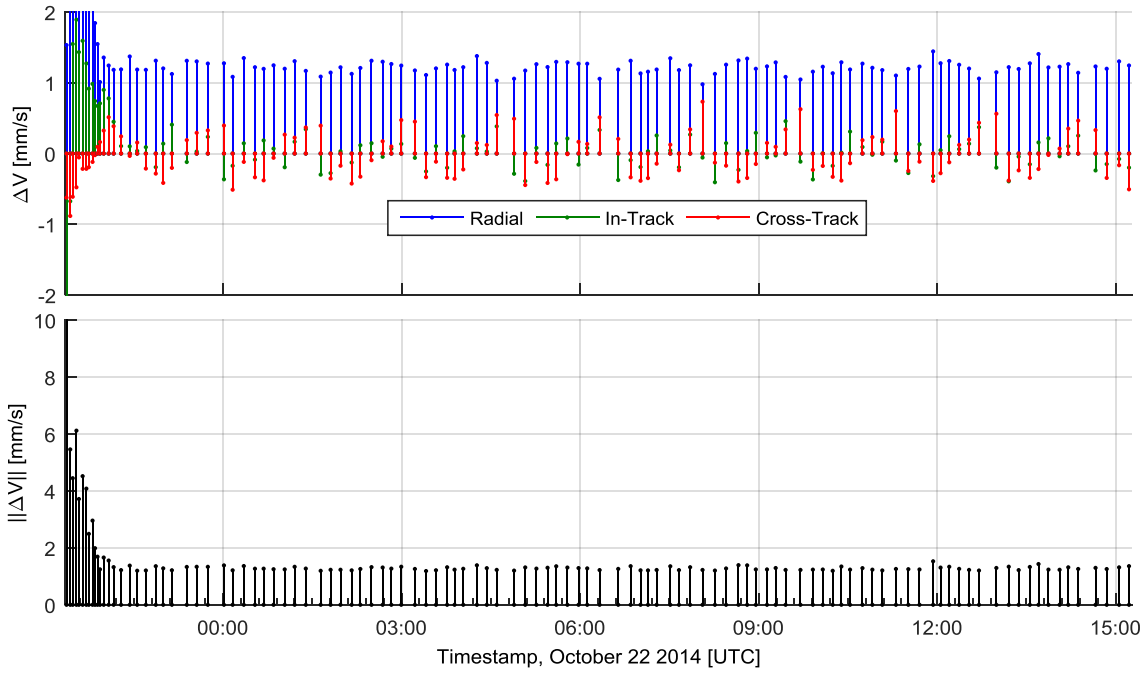

Figure 12. Control Inputs for the 100 m PCO.

The RelNav filter residuals, evaluated offline using the on-orbit solution, are shown in Figure 9. The fact that the sample means are very close to zero with a standard deviation on the order of the expected measurement noise gives some confidence that the filter is functioning correctly. There are also some clearly visible jumps in the magnitude of the filter residuals. These typically surround dynamic events, such as rapid reorientations to align with a new thrust target, as well as thrust events which instantaneously change the spacecraft velocity. It is also common to see a short period with larger residuals following a period of openloop propagation. Upon closer examination of the filter solutions, the position and velocity estimates remain smooth across openloop gaps. It is a sudden change in the differential clock bias estimate which causes the jumps in residual. This is most likely due to the fact that the GPS receivers automatically steer their clocks to GPS time, and thus the clock bias state cannot be accurately predicted in the absence of measurements.

Having succeeded with the ATOs, the PCO experiments were started a few days later. The 100 m PCO reconfiguration error was a little higher than expected, at 14 m and 6.7 mm/s, using 5 cm/s more fuel than expected. The most likely cause of this is an error in the computed control thrust due to a degraded relative navigation solution. Despite this, the LQR was able to reduce the control error below 1 m within 45 minutes, after which the control error stayed well below 1 m for the remainder of the experiment (see Figure 10). It is interesting to note that unlike the ATO formations which show oscillatory errors shared between the radial and in-track directions, there is a constant bias in the radial direction in the PCO control error. This bias is likely due to a mismatch between the controller dynamics and true relative dynamics. The controller formulation assumes an HCW relative motion model, whereas the true relative motion is dominated by differential J_2. The in-plane drift caused by the non-zero differential inclination is not effectively corrected. Furthermore, the control inputs are not as effective as modeled, due to the non-zero eccentricity of the reference orbit. Not including the additional fuel used to establish the formation following reconfiguration, a ΔV of 1.15 cm/s/orbit was required for formation mainte-

nance – roughly 0.15 cm/s/orbit more than predicted. As shown in Figure 11, as with the 500 m ATO, the relative navigation residuals during this formation are consistent with a properly functioning extended Kalman filter. The set of control inputs for this formation is shown in Figure 12. Following the initial convergence a consistent set of thrust inputs are commanded.

The 50 m PCO was completed successfully 9 days later. Following a reconfiguration error of 2 m, the sub-metre control requirement was easily achieved, using (on average) 1.3 cm/s/orbit of fuel – less than half the value predicted in simulation. This improved performance is due to a better-than-predicted relative velocity estimation error.

Following the PCO formations, it was decided to revisit the 1000 m ATO to fully meet the mission requirements. The reconfiguration error upon entering the formation was larger than expected, at 35 m and 4 cm/s. The cause of this is unknown, as there were no apparent relative navigation errors or control thrust implementation errors. The LQR was able to reduce the control error to the sub-metre level within the first orbit, but at the cost of a 26 cm/s fuel penalty. The steady-state fuel consumption was 3.4 cm/s/orbit, just under the predicted value.

Table 4. Fine Formation Flying Control Results Summary.

Formation	$\Delta v_{\text{expected}}$ (cm/s/orbit)	Δv_{actual} (cm/s/orbit)	$\Delta r_{\text{expected}}$ 3D-RMS (cm)	Δr_{actual} 3D-RMS (cm)
ATO 1000	3.65	5.55	59.0	45.3
ATO 500	1.71	1.62	34.5	51.3
PCO 100	0.99	1.63	51.7	60.2
PCO 50	3.07	1.27	55.4	59.4

The formation control accuracy and fuel consumption is summarized in Table 4. Note that the formation control error shown does not include the convergence period between the end of the reconfiguration maneuver and the first point in time the required control error is achieved, whereas the mean fuel consumption does. The sub-metre (2σ) control requirement, interpreted as requiring the 1 m point to fall within the 95.45^{th} percentile, is easily achieved in all cases since the control error magnitude never exceeded 1 m following initial convergence. Where actual fuel consumption is higher than expected, the discrepancy is due to the additional fuel used during the convergence period. In steady state, the actual fuel consumption is much closer to the predicted value. For the 500 m ATO and 50 m PCO, the actual fuel used is lower than expected since the relative velocity estimation error was less on-orbit than in the offline simulation model.

In all, approximately 5 m/s of ΔV was required to complete the mission. Of this, 40% was required for drift recovery following separation from the launch vehicle, 40% for fine formation flying experiments, and 20% for station keeping activities. Between the two spacecraft there is about 75% of the initial ΔV remaining – about 13 m/s for CanX-4 and 7 m/s for CanX-5.

CONCLUSION

The CanX-4 and CanX-5 nanosatellites have completed all high-level mission objectives, having successfully demonstrated autonomous formation flight with control error less than 1 metre in along-track and projected circular formations with a relative range between 1000 m and 50 m. This achievement was enabled by an agile attitude control system, an accurate carrier-phase differential GPS relative navigation algorithm, and reliable two-way communication across the ISL. With this success, it has been shown that operational formation flying missions can be performed with nanosatellites. Currently the spacecraft appear to be in good health and are powered down and drifting slowly relative to one another in wait of their next assignment. Their relative position and phasing is monitored periodically, and maneuvers are applied as required in order to assure

spacecraft safety. Both spacecraft remain available for tasking and have plenty of fuel left over for further formation flying experiments – CanX-5 has more than half its fuel remaining, and CanX-4 should be nearly full.

ACKNOWLEDGMENTS

The authors wish to acknowledge the CanX–4&5 formation flying mission funding sponsors: NSERC, DRDC-Ottawa, CSA, MDA, and Ontario Centres of Excellence. Without their valued contributions, development of this mission would not have been possible. The contributions of Dr. Susan Skone, Dr. Elizabeth Cannon, and Dr. Kyle O'Keefe from the University of Calgary and Dr. Chris Damaren from the University of Toronto are gratefully acknowledged.

REFERENCES

[1] R. Kahle, H. Runge, J.-S. Ardaens, S. Suchandt, R. Romeiser, "Formation flying for along-track interferometric oceanography – First in-flight demonstration with TanDEM-X,", *Acta Astronautica*, vol. 99, pp. 130-142, Jun.-Jul. 2014.

[2] O. Montenbruck, M. Kirschner, S. D'Amico, and S. Bettadpur, "E/I-vector separation for safe switching of the GRACE formation," *Aerospace Science and Technology*, vol. 10, no. 7, pp. 628-635, Oct. 2006.

[3] M. T. Zuber, D. E. Smith, D. H. Leman, T. L. Hoffman, S. W. Asmar, and M. M. Watkins, "Gravity Recovery and Interior Laboratory (GRAIL): Mapping the Lunar Interior from Crust to Core," *Space Science Reviews*, vol. 178, no. 1, pp. 3-24, Sept. 2013.

[4] J. L. Burch, T. E. Moore, R. B. Torbert, and B. L. Giles, "Magnetospheric Multiscale Overview and Science Objectives," *Space Science Reviews*, vol. 199, no. 1, pp. 5-21, Mar. 2016.

[5] D. CaJacob, N. McCarthy, T. O'Shea, and R. McGwier, "Geolocation of RF Emitters with a Formation-Flying Cluster of Three Microsatellites," *Proc. of 30th AIAA/USU Conference on Small Satellites (SmallSat 2016)*, Logan, Utah, August 2016.

[6] S. D'Amico, J.-S. Ardaens, and R. Larsson, "Spaceborne Autonomous Formation-Flying Experiment on the PRISMA Mission," *Journal of Guidance, Control, and Dynamics*, vol. 35, no. 3, pp. 834-850, May-June 2012.

[7] S. Bandyopadhyay, G. P. Subramanian, R. Foust, D. Morgan, S.-J. Chung, and F. Y. Hadaegh, "A Review of Impending Small Satellite Formation Flying Missions," *Proc. of 53rd AIAA Aerospace Sciences Meeting (AIAA SciTech)*, Kissimmee, Florida, January 2015.

[8] J. Z. Newman, "Drift Recovery and Station Keeping for the CanX-4 and CanX-5 Nanosatellite Formation Flight Mission", Master's thesis, University of Toronto, 2015.

[9] K. Sarda, C. C. Grant, M. Chaumont, S. Y. Choi, B. Johnston-Lemke, R. E. Zee, "On-Orbit Performance of the Bright Target Explorer (BRITE) Nanosatellite Astronomy Constellation," *Proc. of 4S Symposium*, Porto Petro, Spain, 26-30 May, 2014.

[10] L. M. Bradbury, N. G. Orr, M. Short, N. Roth, A. Macikunas, B. Kumar, C. Short, B. Ham, and R. E. Zee, "ExactView-9: Commissioning and On-Orbit Operation of a High Performance AIS Nanosatellite," *Proc. of 4S Symposium*, Valletta, Malta, May-Jun. 2016.

[11] A. Beattie, K. Sarda, D. Kekez, R. E. Zee, and B. Narheim, "AISSat-1: In-Orbit Verification of the Generic Nanosatellite Bus," *Proc. of the 62nd International Astronautics Congress*, Cape Town, South Africa, 2011.

[12] S. E. Armitage, L. Stras, G. R. R. Bonin, and R. E. Zee, "The CanX-4&5 Nanosatellite Mission and Technologies Enabling Formation Flight," *Proc. of the 7th International Workshop on Satellite Constellations and Formation Flight*, Lisbon, Portugal, 2013.

[13] B.W. Risi, "Propulsion System Development for the CanX-4 and CanX-5 Dual Nanosatellite Formation Flying Mission," Master's thesis, University of Toronto, 2014.

[14] H. Schaub and J. L. Junkins, *Analytical Mechanics of Space Systems*, 2nd ed. AIAA, 2009.

[15] N. H. Roth, "Navigation and control design for the CanX-4/-5 satellite formation flying mission," Master's thesis, University of Toronto, 2010.

[16] J. Pluym and C. Damaren, "Dynamics and control of spacecraft formation flying: Reference orbit selection and feedback control," *Proc. 13th Canadian Astronautics Conf. (ASTRO 2006)*, Montreal, Quebec, Apr. 2006.

[17] Q. Marji, "Precise relative navigation for satellite formation flying using GPS," Master's thesis, University of Calgary, Jan. 2008.

[18] F. D. Busse, "Precise formation-state estimation in low earth orbit using carrier differential GPS," Ph.D. dissertation, Stanford University, 2003.

[19] T. Ebinuma, "Precision spacecraft rendezvous using global positioning system: an integrated hardware approach," Ph.D. dissertation, University of Texas at Austin, 2001.

[20] O. Montenbruck, T. Ebinuma, E. G. Lightsey, and S. Leung, "A real-time kinematic GPS sensor for spacecraft relative navigation," *Aerospace Science and Technology*, vol. 6, pp. 435–449, 2002.

[21] R. Kroes, "Precise relative positioning of formation flying spacecraft using GPS," Netherlands Geodetic Commission, Tech. Rep. 61, March 2006.

[22] S. Leung and O. Montenbruck, "Real-time navigation of formation-flying spacecraft using global-positioning-system measurements," *Journal of Guidance, Control, and Dynamics*, vol. 28, no. 2, pp. 226–235, March-April 2005.